Composites: Part A 199 (2025) 109215

Contents lists available at ScienceDirect

Composites Part A

journal homepage: www.elsevier.com/locate/compositesa

Defect sensitivity of 2D lattice materials with positive, zero, and negative Poisson's ratios

Xihuan Wang [a], Shuang Hong [a], Yanan Yuan [a], Guoyou Huang [a], Zuoqi Zhang [a,b,*]

[a] Department of Engineering Mechanics, School of Civil Engineering, Wuhan University, Wuhan 430072, PR China
[b] Engineering Research Center on Building Examination and Reinforcement Technology (Ministry of Education), Wuhan University, Wuhan 430071, PR China

HIGHLIGHTS

- Finite element models were established for various lattices with random-distributed missing/broken bars.
- The imperfection sensitivity coefficients were defined to measure and compare the imperfection sensitivity among different lattices.
- Deformation-mode conversion from stretching-dominant to bending-dominant leads to extremely high imperfection-sensitivity.
- Missing-bar defects have crucial effects on Poisson's ratios of 2D lattice materials, especially for the zero and negative types.

GRAPHICAL ABSTRACT

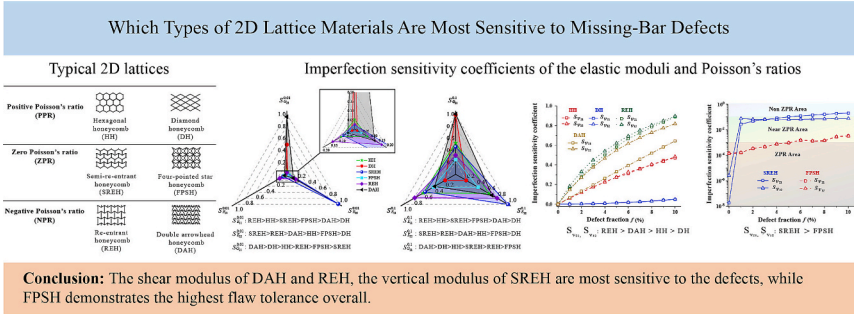

ARTICLE INFO

Keywords:
2D lattice materials
Zero/negative Poisson's ratios
Imperfection sensitivity
Flaw tolerance

ABSTRACT

Two-dimensional (2D) lattice materials with well-designed microstructures exhibit extraordinary properties such as zero and negative Poisson's effects, and play a crucial role in industrial fields. However, inevitable defects from manufacturing, storage, transportation, and service may compromise their microstructures and functionalities. Therefore, it is important but still unclear: which microstructures and associated properties are most or least sensitive to defects. The current study investigated the effects of bar-missing/broken defects on the elastic properties of six typical honeycomb structures—Hexagonal Honeycomb, Diamond Honeycomb, Semi-Re-Entrant Honeycomb, Four-Pointed Star Honeycomb, Re-Entrant Honeycomb, and Double Arrowhead Honeycomb—which are categorized into positive, zero, and negative Poisson's ratio groups. A finite element model incorporating the random distributed defects was developed and the imperfection sensitivity coefficient was defined to quantitatively analyze the sensitivity of elastic properties to missing bars. The results show that the shear modulus of Double Arrowhead Honeycomb and Re-Entrant Honeycomb, and the vertical modulus of Semi-Re-Entrant Honeycomb are most sensitive to the defects, while Four-Pointed Star Honeycomb demonstrates the highest flaw tolerance overall. The underlying mechanisms for defect-sensitivity or flaw-tolerance are closely related to the deformation mode and nodal connectivity of these lattice structures.

* Corresponding author at: Department of Engineering Mechanics, School of Civil Engineering, Wuhan University, Wuhan 430072, PR China.
E-mail address: zhang_zuoqi@whu.edu.cn (Z. Zhang).

https://doi.org/10.1016/j.compositesa.2025.109215
Received 1 July 2025; Received in revised form 23 July 2025; Accepted 30 July 2025
Available online 5 August 2025

1. Introduction

Lattice materials are composed of interconnected bars. By carefully designing different permutations of these bars in regular and periodic arrangements, unique micro-lattice structures are created for specialized functions and applications [1,2]. These materials are valued for their lightweight nature and distinctive mechanical properties such as strong anisotropy and extraordinary Poisson's effects [3,4], and have been widely used in highly demanding engineering environments where conventional materials fall short. Especially, the rapid development and commercialization of additive manufacturing (also well known as 3D printing) technologies has been facilitating the precise productions of lattice materials with more complex microstructures [1,5–7]. However, the elegant and complex microstructure design is usually a double-edged sword: it helps achieve extraordinary properties while reducing robustness and reliability. It is well-known that defects/flaws are inevitable, always accompanying materials/structures throughout their whole life cycle—from manufacturing, to storage, transportation, and application. Thus, important questions arise: How do microstructure flaws affect the mechanical properties of typical lattice materials? Which type of lattice materials and what properties of theirs are most/least sensitive to the flaws? How can we make a quick evaluation on the flaw-sensitivity (or flaw-tolerance) of a lattice design? All these questions are yet to be answered and ask for more systematic and comprehensive research.

Poisson's ratio is an important elastic parameter measuring the ratio of lateral strain to axial strain when a material is uniaxially stretched or compressed. It plays an important role in determining the material's deformation characteristics, stability, and strength. Although its theoretical value ranges from -1 to 0.5, Poisson's ratio of common engineering materials is between 0.1 and 0.5 [8]. However, through microstructure designs in lattice materials, their Poisson's ratios can be engineered beyond the common range of conventional materials, and then the extraordinary properties, functions and applications follow as a result. As illustrated in Fig. 1, six typical two-dimensional (2D) lattice materials are categorized into three groups according to their Poisson's ratios: positive, zero, and negative Poisson's ratios, referred to be PPR, ZPR, and NPR for briefness, respectively. All their periodic unit cell can be determined by three geometric parameters—the bar length l, the bar thickness t, and the tilted angle θ. Hexagonal honeycomb (HH) and diamond honeycomb (DH), as two typical PPR lattice materials, are widely utilized as sandwich core materials in engineering due to their excellent impact resistance and energy absorption capacity [9], such as in the application of fiber reinforced composite honeycomb [5–7,10–14], self-locking structural honeycomb [15], self-folding honeycomb [16] and some hierarchical honeycombs [11,17,18]. ZPR lattice materials including the semi-re-entrant honeycomb (SREH) and four-pointed star honeycomb (FPSH) have numerous applications in aerospace [19–24] and tissue engineering [25–28], in which the material deformation in one direction is desired to be unaffected by the other direction. The re-entrant honeycomb (REH) and double arrowhead honeycomb (DAH) are taken as two typical NPR structures, and have great applications in biomedical engineering, e.g., stents [29–31], cardiac patches [32], wearable device [33,34], bone implant [35–37], since they can provide better compliance to complex surfaces and movements of human organs.

Many studies on the mechanical advantages and applications of these lattice materials can be found in the literature, but few give sufficient attention to their defects. Regarding the defect issue, Gibson, Fleck, and their respective coworkers published several pioneering works in 1990s [39–43]. For example, Gibson and his coworkers investigated the effects of random missing cell walls, cell face curvature, and cell wall corrugations on the mechanical properties of HHs through FEM simulations, and found that the defect existence caused a sharp decrease in the effective mechanical properties [39–42]. Chen et al. (1999) systematically studied the influence of six types of morphological imperfections—waviness, non-uniform cell wall thickness, cell-size variations, fractured cell walls, cell-wall misalignments, and missing cells—on the yielding of HHs by FEM analyses, and concluded that these defects may have knock-down effect on the hydrostatic yield strength due to the defect-induced switch in deformation mode from cell wall stretching to cell wall bending [43]. Followingly, there are an increasing number of studies conducted to probe into more details and more aspects on the topic. Li et al. (2005) conducted a research on the effective Young's modulus and Poisson's ratios of HHs with the defects including Voronoi irregular structures and non-uniform cell walls, and they suggested that the effective Young's modulus is significantly affected by these defects but the Poisson's ratio is not [44]. Symons and Fleck (2008) systematically investigated the effects of missing bars, misplaced nodes, and wavy cell walls on the effective shear moduli and bulk moduli of HHs,

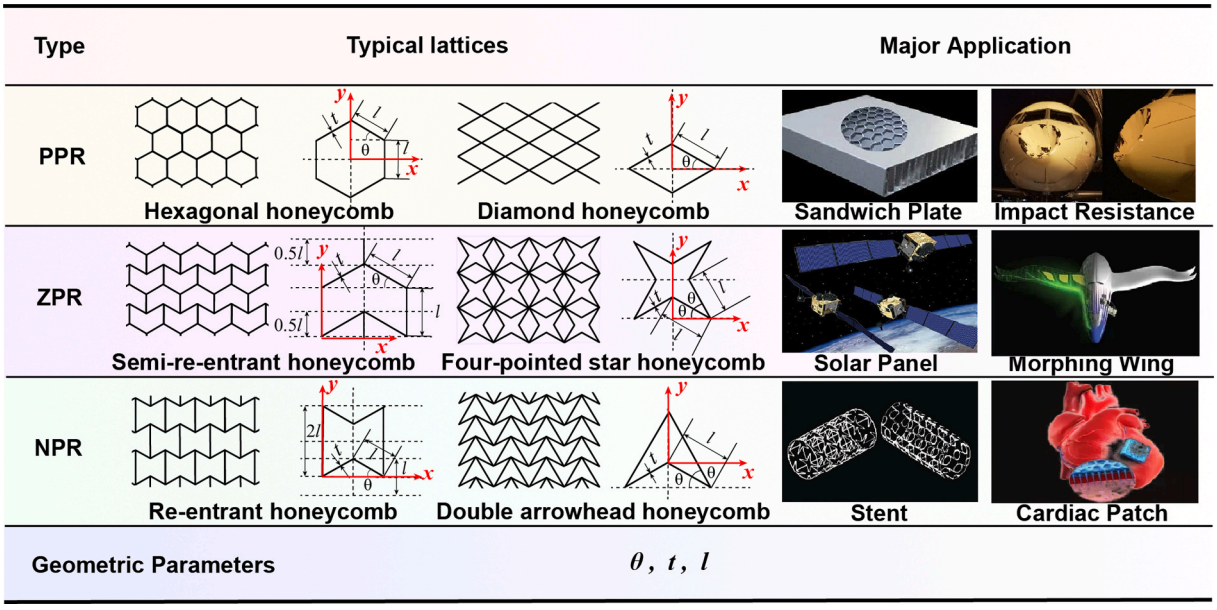

Fig. 1. Typical 2D lattice materials are grouped by their Poisson's ratios: Positive Poisson's ratios (PPR), Zero Poisson's ratios (ZPR), Negative Poisson's ratios (NPR); their major applications are also listed, respectively. (Note: the subpicture on the "stent" is adapted from Ref [38].)

and found that the defects distinctly compromised their bulk moduli but had little effects on their shear moduli [45]. Zhang et al. (2010) analyzed the impact resistance of a metal hexagonal honeycomb with missing cell walls [46]. However, most of these studies focused on the lattice materials of HHs. Romijn and Fleck investigated the imperfection sensitivity of in-plane modulus and fracture toughness for five morphologies of 2D lattice: the isotropic triangular honeycombs, HHs, Kagome lattices, 0/90° squares, and ±45° squares, but their assume imperfection is in form of displaced nodes [47]. Tankasala et al. (2017) studied the finite-strain uniaxial tensile response of 2D elastoplastic lattices including triangular, Kagome, DH, and HH, and the sensitivity of macroscopic ductility and tensile strength to geometric imperfection is also explored by considering the randomly misplaced joints and an array of broken cell walls [48]. Liu et al. (2014) studied the effect of irregularity, residual convex units and stresses on the effective mechanical properties of REH using FEM simulations, and found that the these defects have significant influence on the effective elastic moduli, yield strength, shear moduli, and Poisson's ratio of REH [49]. In summary, most of the existing defect-sensitivity studies mainly focused on HH, insufficient attentions have been paid to other typical lattice structures of PPR, ZPR, and NPR. Moreover, these studies have yet to systematically address the central question we raised here: Which types of lattice materials and what properties of theirs are most/least sensitive to the flaws?

To well address the questions above, the current work systematically conducted FEM simulations to study the influences of random located missing/broken bars on the elastic properties of six lattice structures: HH, DH, SREH, FPSH, REH, and DAH, fully covering three major groups: PPR, ZPR, and NPR. The remaining of the paper is arranged in the following way: the FEM models with the random missing bars are established in Section 2; the results and discussions are presented in Section 3; and, Section 4 gives a summary of the major conclusions.

2. FEM model and verification

FEM simulations were conducted using the widely used commercial software Abaqus (Version 2016). The geometrical models and boundary conditions are illustrated in Fig. 2, with examples of perfect HH subjected to the uniaxial tensile loads along the x and y directions, and the simple shear load in the x-y plane. In the models, a sufficient number of periodic cells are needed to avoid the dispersion of simulation results due to the size or boundary effects, and our trial tests show that 70 periodic cells in each dimension are generally enough, as a result, $70\times70 = 4900$ cells in total. The geometrical parameters in FEM models are all set to be dimensionless and thus the effective moduli acquired from our simulation results are consistent with the Young's moduli of the solid material. All the bars are slender with a square cross-section, the length $l = 1$ (unit length), cross-section edge $t = 0.02$, correspondingly the aspect ratio $\alpha = l/t = 50$. All the tilted angle $\theta = 30°$. The bars are assumed to be rigid-jointed. A 3-node quadratic beam element B32 is adopted for the bars. Mesh converge analysis had been performed to ensure the simulation results to be consistent and reliable before starting systematic simulations, and the element size around 0.05 was finally adopted. All the material parameters of the models are set as those of stainless steel, i.e. $E_s = 209$GPa and $\nu_s = 0.3$. From the FEM simulations, five effective elastic properties can be obtained, specifically, the tensile moduli E_{11} and E_{22}, the Poisson's ratios ν_{12} and ν_{21}, and the shear modulus G_{21}, where subscripts 1 and 2 represent the x and y directions, respectively. In particular, the specific formulae are as follows:

$$E_{11} = \frac{\sigma_{11}}{\varepsilon_{11}} = \frac{F_x/2rL_y}{\Delta_x/L_x} \tag{1}$$

$$\nu_{21} = -\frac{\varepsilon_{22}}{\varepsilon_{11}} = -\frac{\Delta_{yx}/L_y}{\Delta_x/L_x} \tag{2}$$

$$E_{22} = \frac{\sigma_{22}}{\varepsilon_{22}} = \frac{F_y/2rL_x}{\Delta_y/L_y} \tag{3}$$

$$\nu_{12} = -\frac{\varepsilon_{11}}{\varepsilon_{22}} = -\frac{\Delta_{xy}/L_x}{\Delta_y/L_y} \tag{4}$$

$$G_{21} = \frac{\sigma_{21}}{2\varepsilon_{21}} = \frac{F_x/2rL_x}{\Delta_x/L_y} \tag{5}$$

Here L_x and L_y denote the sample dimensions along the x and y directions, respectively; Δ_x represents the uniaxial stretch along the x direction, while Δ_{yx} is the accompanying contraction/expansion in the y direction due to the Poisson's effect; similarly, Δ_y and Δ_{xy} denote the uniaxial stretch along the y direction and the accompanying contraction/expansion in the x direction, respectively. F_x and F_y refer to the resultant reaction forces at the constrained boundaries. $\sigma_{\alpha\beta}$ and $\varepsilon_{\alpha\beta}$ are stress and strain components in the plane, with the subscripts $\alpha, \beta = 1, 2$. Note that G_{12} can also be calculated with analogy to Eq. (5) and $G_{12} = G_{21}$ according to the theory of elasticity.

As mentioned in the previous section, random defects, such as bar missing during the fabrication process or bar broken in the serving stage, are usually inevitable in the whole life cycle of the lattice structures. To this end, randomly distributed defects in forms of missing/broken bars were introduced to the FEM models, and their random locations were assumed to conform to a uniform probability density distribution. Define the defect fraction f as the ratio of the counts of missing/broken bars in the defected structure over the total bar number of its corresponding perfect structure. In the current work, our focus is on the early stage of the lattices' life cycle, for example, the fabrication process, and hence the defect fraction f is limited up to 10 %. All the elements in a defected bar will be killed and deactivated with the element birth and death technique in Abaqus. Ten defect fractions for each lattice, from 1

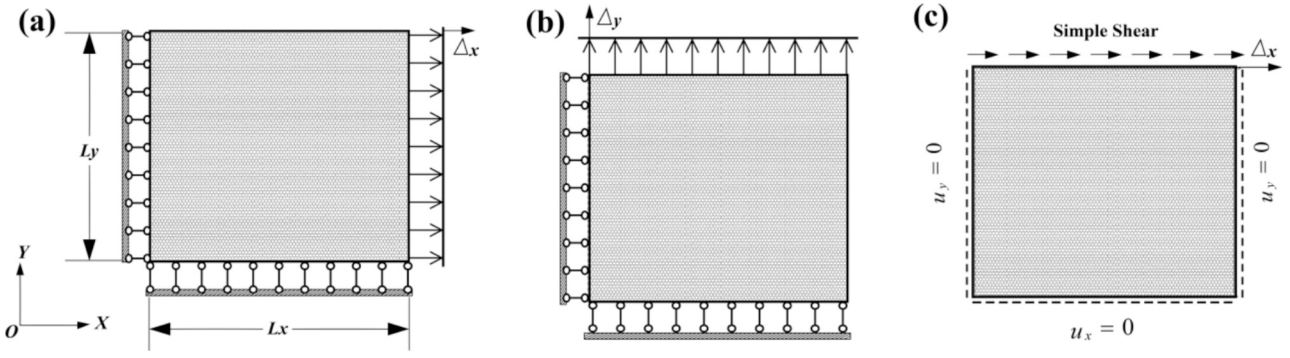

Fig. 2. FEM models for 2D lattice materials under uniaxial tensile or shear loadings: (a) Tension in x direction; (b) Tension in y direction; (c) Simple shear in the x-y plane. Here the perfect hexagonal honeycomb lattice is demonstrated as an example.

% to 10 % with an increment of 1 % in sequence, are considered here. For each defect fraction of each lattice, ten random samples will be generated and simulated, and statistical analyses will be conducted on their results to obtain the mean values and variances of their effective mechanical properties. The random distribution of missing-bar defects is illustrated in Fig. 3 with nine samples that are randomly generated. In the figure, the missing bars are marked as red, and one can see that the missing bars' distributions are roughly uniform.

For perfect status of these lattice structures, there are analytical solutions available for their elastic properties [50–54] (see Appendix A for details), and thus we can verify our FEM models by comparing our simulation results to the theoretical solutions. Fig. 4 shows the comparison for DH as an example, and we can see that the FEM simulation results are in very good agreement with the theoretical solutions. Detailed comparisons for all the six lattices can be found in the Appendix A, and well validate our FEM models. Noteworthy that in perfect state, DH's shear modulus G_{21} (or G_{12}), SREH's tensile modulus E_{22}, and DAH's shear modulus G_{21} (or G_{12}) are two to three orders of magnitude larger than their counterparts. This is because the stretching deformation mode is predominant in these scenarios (see Supplementary Material for the contours of internal forces and moments). The stretching-dominant deformation is much smaller than the bending-dominant deformation, and thus the lattice structures under the stretching-dominant deformation mode are much stiffer [55]. It is also worth noting that HH, FPSH, REH, and DAH in their perfect states demonstrate the same elastic properties in the x and y directions.

3. Results and discussion

In this section, the mean value and variance of the effective mechanical properties of the six lattice structures are analyzed and discussed. The effective elastic moduli are all normalized by their respective counterparts of perfect structures to better compare the defect effect among different moduli and different lattices.

Fig. 5 presents the mechanical properties varying with respect to the defect fraction for typical PPR lattices, i.e., HH and DH. One can see from Fig. 5a that the tensile moduli (E_{11} and E_{22}) and shear moduli G_{21} are all significantly diminished as the defect fraction f increases up to 10 %. It is worth noting that, for both DH and HH, the plots of tensile moduli in the x and y directions are almost the same with each other, indicating that the defect effects on the tensile modulus are independent on the directions. The tensile and shear moduli of HH and the tensile moduli of DH all decrease in a linear way, but the decease slope for HH's tensile moduli is largest, that for DH's tensile moduli is smallest, and that for HH's shear modulus is between them. In particular, when the defect fraction reaches 10 %, the HH's tensile moduli are reduced by about 63 %, the HH's shear modulus is reduced by about 52 %, whereas the DH's tensile moduli are just by about 20 %. These indicate that the tensile and shear moduli of HH are quite sensitive to the defects, while the tensile moduli of DH are not so sensitive. In contrast, the shear modulus of DH exponentially decreases with the increasing defect fraction. Even just 1 % of defects are introduced, the DH shear modulus significantly drops by about 48 %, and it becomes close to zero (i.e., completely loss of shear load resistance) when the defect fraction reaches 10 %. This suggests that the DH shear property is extremely sensitive to the defects. Noteworthy that the DH's shear modulus is several orders in magnitude higher than others (see Table 1 in Appendix A), but the advantage seems not robust in the presence of imperfections. The mechanism lies in its deformation mode transformation: DH under shear loadings is stretching dominated in its perfect state and thus very stiff, while the presence of bar-missing imperfections induces the conversion of deformation mode from stretching-dominant to bending-dominant and hence become softened significantly [53,55]. The defect-induced deformation mode transformation can be evidenced by the contours of

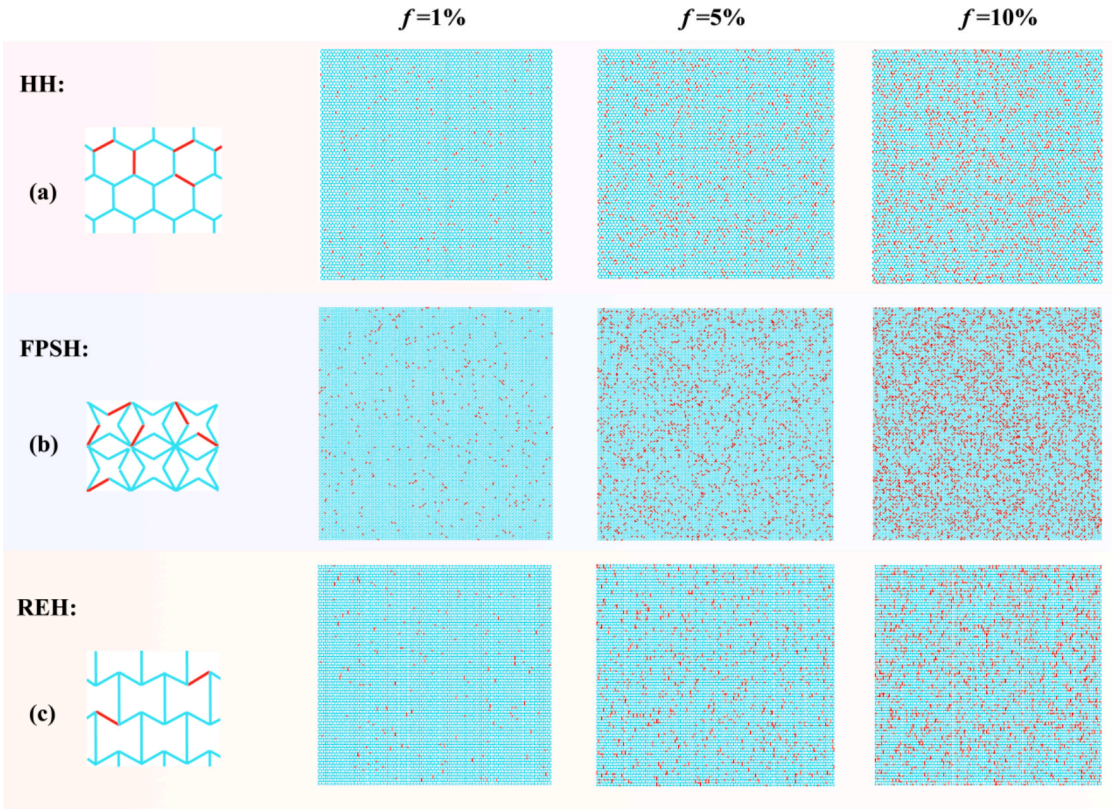

Fig. 3. Illustrations of the random distribution of missing-bar defects: Three defect fractions $f = 1$ %, 5 %, and 10 % are shown, respectively, for each representative lattice: (a) Hexagonal honeycomb (HH), (b) Four-pointed star honeycomb (FPSH), and (c) Re-entrant honeycomb (REH). Note that the missing bars are randomly distributed, conforming to a uniform probability density distribution.

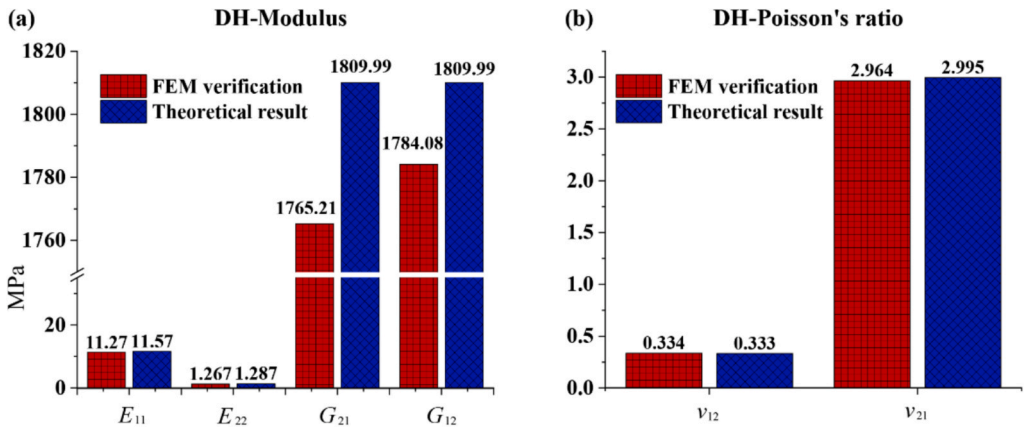

Fig. 4. Justification of our FEM models by comparing with the theoretical results: (a) the tensile moduli E_{11} and E_{22}, and the shear modulus G_{21}; (b) Poisson's ratios ν_{12} and ν_{21}. Here the diamond honeycomb (DH) is demonstrated as an example.

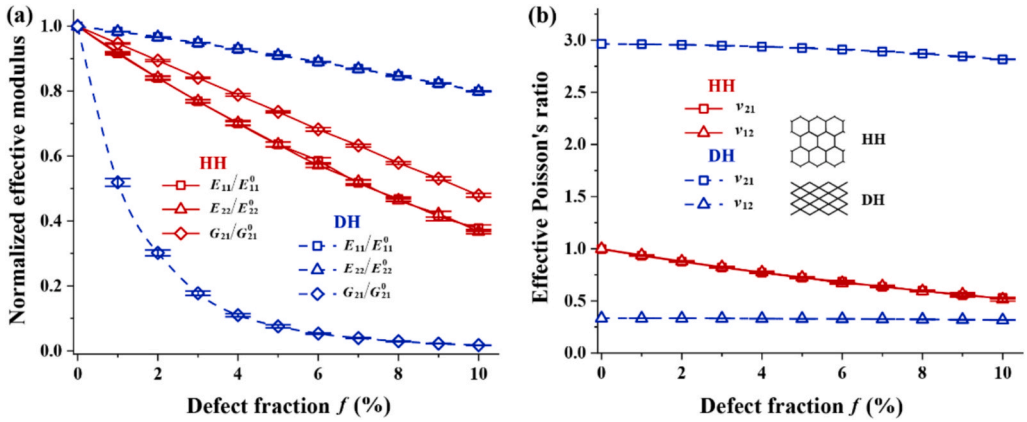

Fig. 5. The mechanical properties varying with respect to the missing-bar fraction for typical PPR lattices: (a) Normalized moduli E_{11}/E_{11}^0,E_{22}/E_{22}^0, and G_{21}/G_{21}^0 by their respective counterparts of perfect lattices; (b) Poisson's ratios ν_{12} and ν_{21}.

internal forces and moments in Supplementary Material. Fig. 5b shows the effective Poisson's ratios of HH and DH varying with the defect fraction. It can be seen that the plots for ν_{21} and ν_{12} of HH are completely overlapped and gradually decrease from 1.0 with the perfect structure to about 0.5 with the defect fraction of 10 %. For DH, ν_{12} and ν_{21} are different from each other: for the perfect lattice, ν_{21} has a value about 2.99 while ν_{12} is about 0.33; as the defect fraction increases to 10 %, ν_{21} and ν_{12} just have a little bit decrease, respectively, from 2.99 to 2.81 and from 0.33 to 0.32. Thus, it can be inferred that DH is less sensitive than HH in Poisson's ratios

The decreases of mechanical properties with respect to the increasing defect fraction for typical ZPR lattices, i.e., SREH and FPSH, are plotted in Fig. 6. The microstructural features evidently tell that the mechanical properties of FPSH are the same in the x and y directions, while they are different for SREH. The simulation results are in good agreement with the predictions. As the defect fraction increases up to 10 %, E_{11}, E_{22} and

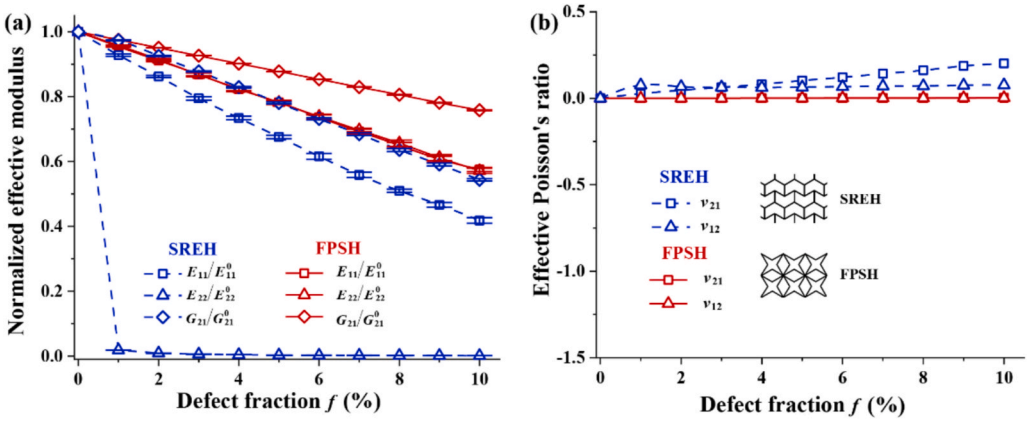

Fig. 6. The mechanical properties varying with respect to the missing-bar fraction for typical ZPR lattices: (a) Normalized moduli E_{11}/E_{11}^0,E_{22}/E_{22}^0, and G_{21}/G_{21}^0 by their respective counterparts of perfect lattices; (b) Poisson's ratios ν_{12} and ν_{21}.

G_{21} of FPSH and E_{11} and G_{21} of SREH gradually decrease in a linear fashion. When the defect ratio f increases to 10 %, FPSH's G_{21} is reduced by about 24 % while its E_{11} and E_{22} is reduced by about 43 %. This suggests that FPSH's shear properties are more robust than its tensile properties when microstructure imperfections are present. For SREH, its G_{21} and E_{11} are respectively reduced by about 46 % and 58 % when f reaches 10 %, significantly larger than their counterparts of FPSH. Moreover, SREH's E_{22} is especially sensitive to the microstructure imperfection, whose value drops by about 98 % even at a small percentage of defect fraction $f = 1$ %. With the defect fraction beyond 2 %, SREH almost completely loses its capability to bear tensile loads in the y direction. Thus, it can be inferred that SERH is generally more sensitive to the imperfection than FPSH in terms of tensile and shear moduli. Furthermore, the similar conclusion can be drawn about effective Poisson's ratios from Fig. 6b. We can see that as the defect fraction varies from 0 to 10 %, the effective Poisson's ratios of FPSH remain zero, whereas for SREH ν_{12} slightly deviates upward from zero and ν_{21} deviates more than ν_{12}. It is worth mentioning that SREH's E_{22} that is most fragile to imperfections. This is also owing to the imperfection-induced conversion from stretching-dominated deformation mode to bending-dominated deformation mode (see Supplementary Material), with analogy to the case of DH's G_{21}.

Fig. 7 presents the plots of mechanical properties varying with respect to the defect fraction for typical NPR lattices, i.e., REH and DAH. One can observed that most of their mechanical indices decrease in nonlinear way with respect to the increasing of defect fraction. G_{21} of REH and E_{11} of DAH gradually decline with the defect fraction, and their respective reductions are about 33 % and 40 % until the defect fraction reaches 10 %. E_{22} of DAH and E_{11} and E_{22} of REH decline much faster, and are reduced by 70 %, 78 %, and 79 %, respectively, when the defect fraction gets up to 10 %. G_{21} of DAH decreases fastest and drops by more than 95 % even just with 1 % of defects. The effective Poisson's ratios are seen significantly increasing from around -1.0 up to -0.1, as the defect fraction increases to 10 %. It is worth noting that REH exhibits the same varying trend in the mechanical properties along the x and y directions, just as indicated by the analytical solutions for its perfect state [50,51]. In contrast, the mechanical properties along the x and y directions for DAH become significantly different due to the presence of imperfections. In addition, DAH's G_{21} that is one of the best mechanical performances shown in Table 1 in Appendix A owing to its stretching-dominant deformation mode, is also most fragile to imperfections, with analogy to DH's G_{21} and SREH's E_{22} (see Supplementary Material).

HH, SREH, and REH have a close relationship in the microstructure. SREH and REH can be regarded as variations of HH to achieve the conversion from positive Poisson's ratio to zero and negative Poisson's ratio, respectively. Thus, it is interesting to make an imperfection-sensitivity comparison among them. Fig. 8a demonstrates the plots of tensile and shear moduli varying with respect to the defect fraction for HH, SREH, and REH. Regarding the shear modulus G_{21}, HH's curve declines fastest, REH's declines slowest, and SREH's is sandwiched by them. It suggests that the imperfection sensitivity of shear modulus decreases from HH to SREH, and REH, in sequence. With respect to the tensile modulus E_{11}, the sequence of their imperfection sensitivity from high to low is REH, HH, and SREH, different from that for the shear modulus. However, the curves for HH and SREH are close to each other. In terms of the tensile modulus E_{22}, the curve of HH declines slowest, that of SREH declines fastest, and that of REH is between them. As aforementioned, SREH's E_{22} exhibits a quick drop as the defect fraction increases from 0 to 1 %. Fig. 8b shows the plots of Poisson's ratios varying with respect to the defect fraction for HH, SREH, and REH. One can see that the curves of ν_{21} and ν_{12} for each lattice structure are close to each other. Interestingly, the positive Poisson's ratios (HH) gradually decrease, the negative Poisson's ratios (REH) gradually increase, while the zero Poisson's ratios (SREH) keep around zero, as the defect fraction increases up to 10 %. It can be inferred from the structural features that the positive/negative Poisson's ratio originates from the inward/outward rotation of the inclined bars under tensile loadings. As the number of missing bars increases, the inclined bars are reduced and so their rotation effects will be reduced accordingly. When the defect fraction reaches 10 %, HH and REH are still located in their own category, PPR and NPR, respectively; however, SREH has been shifted out of the ZPR zone. The special ranges or categories of Poisson's ratios such ZPR and NPR are crucially important to specific engineering applications of these lattice materials, and hence much more attention should be paid to the change of Poisson's ratios with the presence of structural imperfections.

The results above tell that the missing-bar defects have effects of different degree on the mechanical properties of these lattice materials. To quantitatively measure and compare the imperfection sensitivity of these lattices, the imperfection sensitivity coefficient at any specific defect fraction is defined as below:

$$S_Y^f = \frac{Y_0 - Y_f}{Y_0} \tag{6}$$

where the subscript Y represents the effective properties such as E_{11}, E_{22} and G_{21}, while the superscript fraction is the defect fraction f. However, it is a little complicated for Poisson's ratios, especially considering the ZPR lattices of great interest here. Thus, the imperfection sensitivity coefficient for Poisson's ratio is adapted to be:

$$S_Y^f = \begin{cases} |Y_0 - Y_f|, & Y_0 \in (-0.001, 0.001); \\ \left|\dfrac{Y_0 - Y_f}{Y_0}\right|, & \text{otherwise} \end{cases} \tag{7}$$

where Y represents ν_{21} or ν_{12}. The adaptation can well avoid dividing by

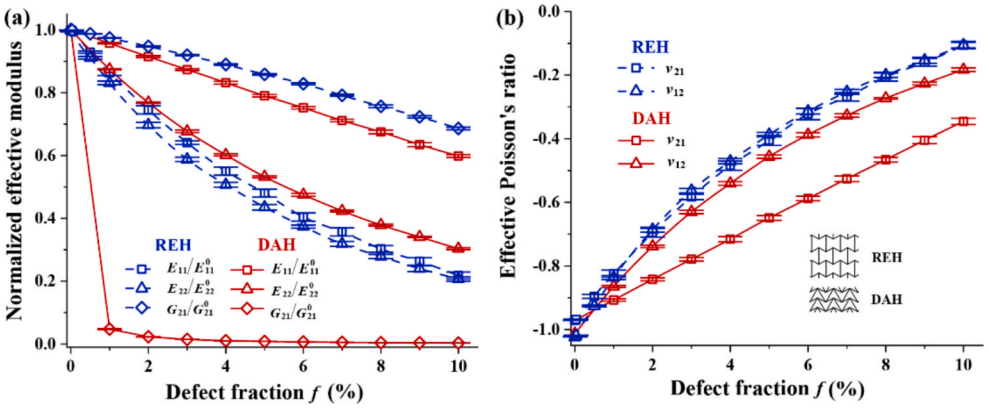

Fig. 7. The mechanical properties varying with respect to the missing-bar fraction for typical NPR lattices: (a) Normalized moduli E_{11}/E_{11}^0,E_{22}/E_{22}^0, and G_{21}/G_{21}^0 by their respective counterparts of perfect lattices; (b) Poisson's ratios ν_{12} and ν_{21}.

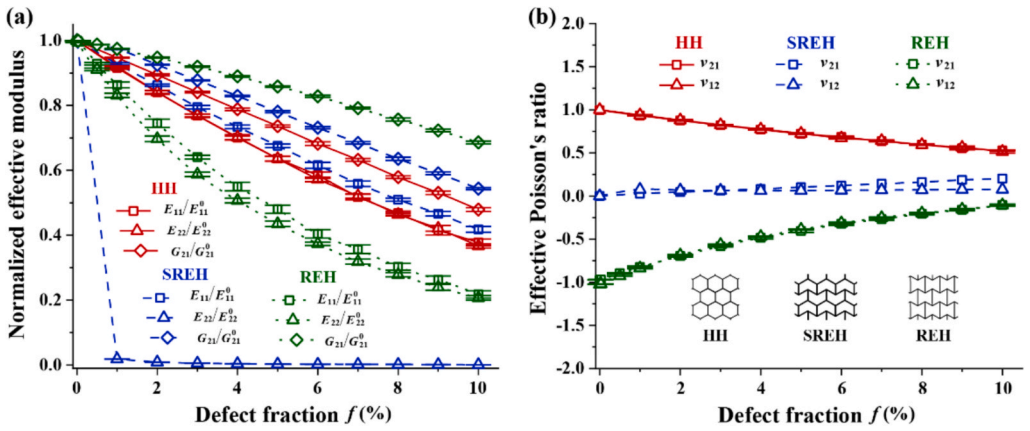

Fig. 8. Comparison among the three typical hexagonal variations: namely, hexagonal, semi-re-entrant, and re-entrant honeycomb: (a) Normalized moduli E_{11}/E_{11}^0,E_{22}/E_{22}^0, and G_{21}/G_{21}^0 by their respective counterparts of perfect lattices; (b) Poisson's ratios ν_{12} and ν_{21}.

zero in the ZPR scenario. It is noteworthy that there is still no specific definition about the ZPR materials of practical interest in literature, and here we limit the Poisson's ratios of ZPR materials in the range between -0.001 and 0.001, at least two orders of magnitude less than the common values of conventional engineering materials (0.1∼0.5). Generally speaking, the imperfection sensitivity coefficients are defined as the percentage of mechanical degradation of defected lattices with comparison to their perfect states, except that the absolute change in Poisson's ratios is adopted for the ZPR lattices.

Fig. 9 summarizes the imperfect sensitivity coefficients of elastic moduli for the six lattice structures with spider charts. Two typical defect fractions 1 % and 10 % were adopted to represent the influence of relatively small and large fractions, respectively. The detailed data are also presented in Table A2 in Appendix B. Fig. 9a shows that $S_{E_{22}}^{0.01}$ for SREH and $S_{G_{21}}^{0.01}$ for DAH are close to one, and $S_{G_{21}}^{0.01}$ for DH is about 49 %, indicating that they are extremely sensitive to the missing-bar imperfection and even a small fraction of missing bars may lead to severe deterioration in these terms of these lattices. Nonetheless, $S_{E_{11}}^{0.01}$ and $S_{E_{22}}^{0.01}$ just around 1.6 %, are the smallest among the coefficients in Fig. 9a, reflecting that they are least sensitive to the imperfections. In another word, they are most tolerant to the flaws. It is also worth noting that all the imperfection sensitivity coefficients of FPSH ($S_{E_{11}}^{0.01}$, $S_{E_{22}}^{0.01}$, and $S_{G_{21}}^{0.01}$) in Fig. 9a are smaller than 4.6 %. This means FPSH has the best overall flaw-tolerant capability in terms of the elastic moduli. Other imperfection sensitivity coefficients are around 10 %, showing a moderately sensitive to the imperfection when the defect fraction is small. At the defect fraction $f = 10$ % (see Fig. 9b), all the imperfection sensitivity coefficients go beyond 20 %, that evidently shows the unignorable mechanical deterioration due to the presence of large fraction of missing bars. Especially, $S_{E_{22}}^{0.1}$ for SREH, $S_{G_{21}}^{0.1}$ for DH and DAH, $S_{E_{11}}^{0.1}$ and $S_{E_{22}}^{0.1}$ for REH are all larger than 70 %, suggesting that their poor flaw-tolerance at the relatively large defect fraction. Overall, FPSH still performs best in the flaw-tolerant capability at the large defect fraction of 10 %.

As aforementioned, the imperfection-induced stretching-to-bending conversion of deformation mode is mainly responsible for the extreme imperfection sensitivity in E_{22} of SREH, and G_{12} of DH and DAH. In terms of microstructure feature, the imperfection sensitivity of a lattice structure is closely related to its degree of nodal connectivity Z, i.e., the number of bars attached to each node [45]. According to Maxwell's equation for the rigidity of lattice structures [56], the necessary but not sufficient condition for rigidity of a two-dimensional lattice is $Z \geq 4$. Similar principles are also revealed for fiber networks [57]. For HH, SREH, and REH, $Z = 3$ in their perfect states; due to their low nodal connectivity, they are usually flexible and bending dominated in deformation, except the special scenario of SREH subjected to tensile loading in the y direction [53]. However, the stretching-dominated mode of SREH is elegant and prone to break down once structural

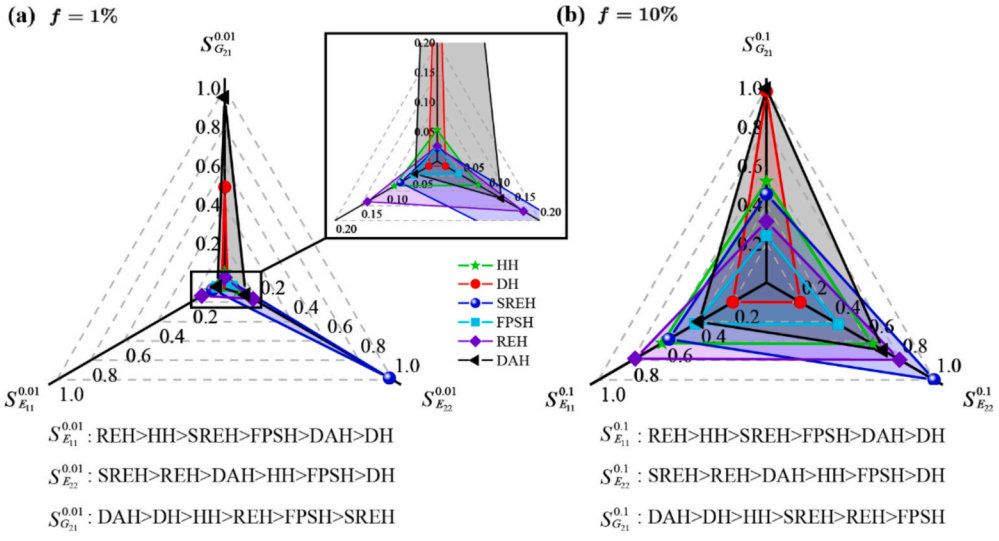

Fig. 9. Spider charts showing the missing-bar sensitivities of the six typical lattices: Missing-bar fraction of 1 % (a), and 1 % (b).

imperfections come into effect. Thus, we can see that SREH's E_{22} is extremely sensitive to bar-missing defects. For DH and DAH, $Z = 4$, just meeting the necessary condition. While most of them in perfect state are bending-dominant, their perfect structures under shear loadings are stretching-dominant and thus very stiff. For FPSH, $Z = 8$ at inter-star nodes while $Z = 2$ at intra-star nodes. It is obvious that the inter-star nodes are more important for loading transfer among stars. Nevertheless, the perfect FPSH is bending-dominant regardless of tensile or shear loadings. For these bending-dominant structures and loading conditions in their perfect states, there are no conversions from stretching-dominant to bending-dominant deformation mode so that no abrupt drops in the corresponding mechanical properties occur when bar-missing imperfections come into effect. Furthermore, for the lattice structures with larger Z, a small portion of bars missing have little effect on the loading transfer mode and efficiency among nodes, and hence they are imperfection insensitive when the imperfection fraction is very small (e.g., less than 1 %). This can somehow explain why FPSH generally performs best in imperfection insensitivity or flaw-tolerant capability.

Fig. 10a shows the missing-bar sensitivity of Poisson's ratios varying with the defect fraction for PPR and NPR lattices, while Fig. 10b is for the ZPR lattices. The detailed data for two typical defect fractions 1 % and 10 % are also presented in Table A3 in Appendix B. For the PPR and NPR lattices (see Fig. 10a), the imperfection sensitivity coefficients gradually increase with the defect fraction. NPR's curves are above those of PPR lattices, suggesting that NPR lattices are more sensitive to the bar-missing imperfections than PPR lattices. The imperfection sensitivity decreases in the sequence: REH, DAH, HH, and DH. At the defect fraction $f = 1$ %, their imperfection sensitivity coefficients are 0.1516, 0.0657, 0.0637, 0.0011 for ν_{21} and 0.1833, 0.1468, 0.0605, 0.0011 for ν_{12} in sequence. At the defect fraction $f = 10$ %, their imperfection sensitivity coefficients increase to be 0.8913, 0.6442, 0.4698, 0.0500 for ν_{21} and 0.8968, 0.8196, 0.4847, 0.0509 for ν_{12} in sequence, respectively. For ZPR lattices (see Fig. 10b), FPSH is distinctly less sensitive to the imperfection than SREH. FPSH always stays in the ZPR category (Poisson's ratio$\leq 10^{-3}$) until the defect fraction reaches $f = 5$ %, beyond which FPSH is still near the ZRP category (Poisson's ratio$\leq 10^{-2}$) up to 10 % of defect fraction. In contrast, SREH has gone out of the ZPR category and got Poisson's ratios around 0.1, even when the defect fraction is as small as $f = 1$ %. It is interesting to mention that negative and zero Poisson's ratios are highly dependent on the elegant design of *meta*-structures, and are prone to reverting to positive Poisson's ratios, which are more natural in common materials. Moreover, ZPR and NPR are crucial for some engineering applications under extreme conditions, and therefore special attention must be paid to the change of Poisson's ratios with the presence of structural imperfections or damages.

4. Conclusions

Centered around the question, which types of 2D lattice materials are most/least sensitive to missing-bar defects, the present paper systematically investigated the effects of bar-missing/broken defects on the elastic properties of six typical honeycomb structures—hexagonal honeycomb (HH), diamond honeycomb (DH), semi-re-entrant honeycomb (SREH), four-pointed star honeycomb (FPSH), re-entrant honeycomb (REH), and double arrowhead honeycomb (DAH)— which are categorized into positive, zero, and negative Poisson's ratio groups (PPR, ZPR, and NPR for briefness). A finite element model (FEM) incorporating the random distributed defects is developed and the imperfection sensitivity coefficient is defined to quantitatively analyze the sensitivity of key elastic properties, including effective Young's modulus, Poisson's ratio, and shear modulus, to missing bars. The major conclusions below are drawn:

(1) 2D lattice materials that have low nodal connectivity (e.g., around 4) and are stretching-dominant (under specific loading modes) in their perfect states are most sensitive to missing-bar defects, since the presence of defects leads to the deformation mode conversion of stretching-dominant to bending-dominant and results in a sharp drop in the stiffness. DH's G_{12}, SREH's E_{22}, and DAH's G_{12} in the current study are just such cases.
(2) Conversely, 2D lattice materials that have high nodal connectivity and are bending-dominant in their perfect states are most insensitive to missing-bar defects, because there are no imperfection-induced deformation mode conversion and a small portion of bars missing have little effect on the loading transfer mode and efficiency among nodes. FPSH in the current study is just the case.
(3) Regardless of the types of 2D lattice materials, all the elastic moduli are reduced significantly (more than 20 %) when the defect fraction goes up to 10 %. It clearly indicates the unignorable mechanical deterioration due to the presence of large fraction of missing bars.
(4) Missing-bar defects have sound effects on Poisson's ratios of 2D lattice materials, especially for NPR and ZPR types. Negative and zero Poisson's ratios are highly dependent on the elegant design of *meta*-structures, and are prone to reverting to positive Poisson's ratios once the *meta*-structures break down. This calls for special caution for the engineering applications that utilize the NPR and ZPR characteristics of 2D lattice materials.

This work shows the comparative advantages and disadvantages of typical lattice materials (covering six types and three categories of Poisson's ratios) in the mechanical sensitivity to defects, and unveils the principal mechanisms of their defect-sensitivity or flaw-tolerance in

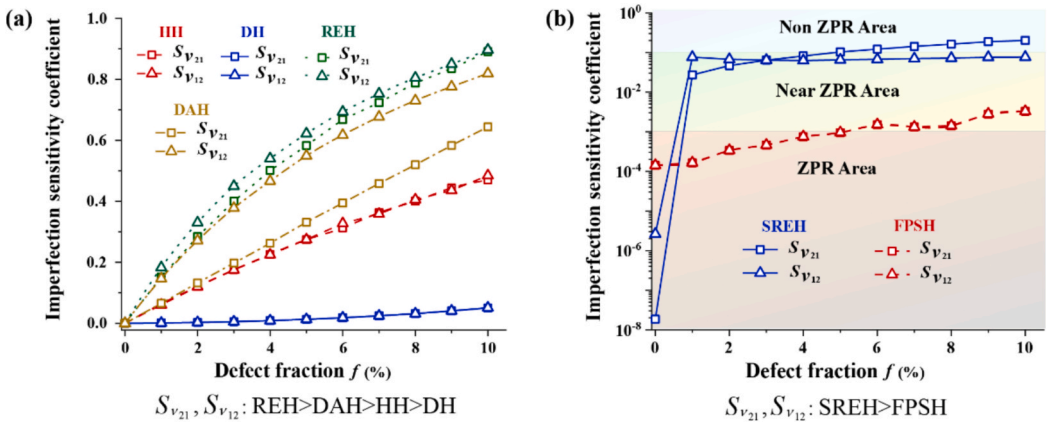

Fig. 10. Comparison of the missing-bar sensitivity of Poisson's ratios among the six typical lattices: (a) PPR and NPR lattices; (b) ZPR lattices.

relation to their structure features. These findings and conclusions may serve as useful guidelines for the selection, optimization, fabrication control, and safety evaluation of functional lattice materials. Nevertheless, it is worth noting that the current study only focused on the bar-missing defects and the elastic properties. Some other forms of defects such as dimensional deviation and surface roughness and more complicate mechanical behaviors including fracture and crashworthiness are also of high importance for the practical fabrication and application of lattice materials. These issues are all great topics for future studies in this field.

CRediT authorship contribution statement

Xihuan Wang: Writing – original draft, Validation, Methodology, Investigation. **Shuang Hong:** Writing – review & editing, Visualization. **Yanan Yuan:** Writing – review & editing. **Guoyou Huang:** Writing – review & editing. **Zuoqi Zhang:** Writing – review & editing, Supervision, Project administration, Methodology, Funding acquisition, Conceptualization.

Declaration of competing interest

The authors declare that they have no known competing financial interests or personal relationships that could have appeared to influence the work reported in this paper.

Acknowledgements

The work was supported by National Natural Science Foundation of China (Grant Nos. 12272279, 11720101002, 11772240), Key R&D Plan Projects of Hubei Province (No. 2021BCA106), and the Fundamental Research Funds for the Central Universities (2042024kf0034).

Appendix A. Verification of FEM model

Table A1 shows the FEM results of elastic properties for the six types of lattice materials, along with the theoretical results for comparison purpose. The details of the theoretical models can be found in Refs.[50–54]. For completeness and ease of reference, the formulae are listed below.

For HH [51]:

$$E_{11} = E_s\left(\frac{t}{l}\right)^3 \frac{\cos\theta}{(1+\sin\theta)\sin^2\theta} \tag{A.1}$$

$$\nu_{21} = \frac{\cos^2\theta}{(1+\sin\theta)\sin\theta} \tag{A.2}$$

$$E_{22} = E_s\left(\frac{t}{l}\right)^3 \frac{1+\sin\theta}{\cos^3\theta} \tag{A.3}$$

$$\nu_{12} = \frac{(1+\sin\theta)\sin\theta}{\cos^2\theta} \tag{A.4}$$

$$G_{21} = E_s\left(\frac{t}{l}\right)^3 \frac{1+\sin\theta}{3\cos\theta} \tag{A.5}$$

For DH [53,54]:

$$E_{11} = \frac{E_s\cos\theta}{\alpha\sin\theta(\alpha^2-(\alpha^2-1)\cos^2\theta)} \tag{A.6}$$

$$\nu_{21} = \frac{(1-\alpha^2)\cos^2\theta}{(\alpha^2-1)\cos^2\theta-\alpha^2} \tag{A.7}$$

$$E_{22} = \frac{E_s\sin\theta}{\alpha\cos\theta(1+(\alpha^2-1)\cos^2\theta)} \tag{A.8}$$

$$\nu_{12} = \frac{(\alpha^2-1)\sin^2\theta}{1+(\alpha^2-1)\cos^2\theta} \tag{A.9}$$

$$G_{21} = \frac{E_s\cos\theta\sin\theta}{\alpha} \tag{A.10}$$

When the aspect ratio $\alpha = l/t$ is much larger than 1, the formulae are simplified to be:

$$E_{11} = E_s\left(\frac{t}{l}\right)^3 \frac{\cos\theta}{\sin^3\theta} \tag{A.11}$$

$$\nu_{21} = \frac{\cos^2\theta}{\sin^2\theta} \tag{A.12}$$

$$E_{22} = E_s\left(\frac{t}{l}\right)^3 \frac{\sin\theta}{\cos^3\theta} \tag{A.13}$$

$$\nu_{12} = \frac{\sin^2\theta}{\cos^2\theta} \tag{A.14}$$

$$G_{21} = E_s\left(\frac{t}{l}\right)\cos\theta\sin\theta \tag{A.15}$$

For SREH [53]:

$$E_{11} = \frac{E_s\cos\theta}{\alpha(\alpha^2-(\alpha^2-1)\cos^2\theta)} \tag{A.16}$$

$$E_{22} = \frac{E_s((\alpha^2-1)\cos^2\theta-\alpha^2)}{(2\alpha^3-2\alpha)\cos^3\theta-3\alpha^3\cos\theta} \tag{A.17}$$

$$\nu_{21} = \nu_{12} = 0 \tag{A.18}$$

$$G_{21} = \frac{E_s\cos\theta(7\alpha^2\cos^2\theta-\cos^2\theta+1)}{(21\alpha^5-10\alpha^3+\alpha)\cos^4\theta+(17\alpha^3-2\alpha)\cos^2\theta+\alpha} \tag{A.19}$$

When the aspect ratio $\alpha = l/t$ is much larger than 1, the formulae above are simplified to be:

$$E_{11} = E_s\left(\frac{t}{l}\right)^3\frac{\cos\theta}{\sin^2\theta} \tag{A.20}$$

$$E_{22} = E_s\left(\frac{t}{l}\right)\frac{\sin^2\theta}{3\cos\theta-2\cos^3\theta} \tag{A.21}$$

$$\nu_{21} = \nu_{12} = 0 \tag{A.22}$$

$$G_{21} = E_s\left(\frac{t}{l}\right)^3\frac{1}{3\cos\theta} \tag{A.23}$$

For FPSH [52]:

$$E_{11} = E_{22} = \frac{E_s}{\alpha^3\sin^2\theta+\alpha\cos^2\theta} \tag{A.24}$$

$$\nu_{21} = \nu_{12} = 0 \tag{A.25}$$

$$G_{21} = \frac{E_s}{8\alpha^3\cos^2\theta} \tag{A.26}$$

When the aspect ratio $\alpha = l/t$ is much larger than 1, the formulae above are rewritten to be:

$$E_{11} = E_{22} = E_s\left(\frac{t}{l}\right)^3\frac{1}{\sin^2\theta} \tag{A.27}$$

$$\nu_{21} = \nu_{12} = 0 \tag{A.28}$$

$$G_{21} = E_s\left(\frac{t}{l}\right)^3\frac{1}{8\cos^2\theta} \tag{A.29}$$

For REH [50,51]:

$$E_{11} = E_s\left(\frac{t}{l}\right)^3\frac{\cos\theta}{(2-\sin\theta)\sin^2\theta} \tag{A.30}$$

$$\nu_{21} = -\frac{\cos^2\theta}{(2-\sin\theta)\sin\theta} \tag{A.31}$$

$$E_{22} = E_s\left(\frac{t}{l}\right)^3\frac{2-\sin\theta}{\cos^3\theta} \tag{A.32}$$

$$\nu_{12} = -\frac{(2-\sin\theta)\sin\theta}{\cos^2\theta} \tag{A.33}$$

$$G_{21} = E_s\left(\frac{t}{l}\right)^3\frac{2-\sin\theta}{20\cos\theta} \tag{A.34}$$

For DAH [54]:

$$E_{11} = E_s\left(\frac{t}{l}\right)^3\frac{\tan^2 2\theta\cos\theta+\tan^2\theta\cos 2\theta}{\cos^3\theta\tan^2 2\theta\tan^2\theta(\tan 2\theta-\tan\theta)} \tag{A.35}$$

$$\nu_{21} = \frac{-1}{\tan 2\theta \tan\theta} \tag{A.36}$$

$$E_{22} = E_s \left(\frac{t}{l}\right)^3 \frac{\tan^2 2\theta \cos\theta + \tan^2\theta \cos 2\theta}{\cos^3\theta(\tan 2\theta - \tan\theta)} \tag{A.37}$$

$$\nu_{12} = -\tan 2\theta \tan\theta \tag{A.38}$$

Adopting $l = 1$, $t = 0.02$ (correspondingly the aspect ratio $\alpha = l/t = 50$), $E_s = 209\text{GPa}$, $\nu_s = 0.3$ (ν_s contributes little to the effective elastic modulus here), and $\theta = 30^\circ$, the formulae provide the theoretical results in Table A1.

In the formulae above, the moduli are proportional to $\left(\frac{t}{l}\right)$, usually indicating that they are high and correspond to the stretching-dominant deformation mode; on the contrary, the moduli are proportional to $\left(\frac{t}{l}\right)^3$, usually suggesting that they are low and correspond to the bending-dominant deformation mode. Then, we inferred that DH's G_{21} and SREH's E_{22} are stretching-dominated mechanical properties and should be relatively large. It is also noteworthy that the analytical solution for the effective shear moduli of DAH is not available in the literature. It's anticipated that the effective shear moduli of DAH should be relatively large, since DAH and DH have some similarity in geometric topology.

Table A1
The comparison between the numerical and analytical solution of the effective properties of six lattice structures.

Lattice		Method	E_{11} (MPa)	E_{22} (MPa)	ν_{12}	ν_{21}	G_{12} (MPa)	G_{21} (MPa)
PPR	HH	FEM	3.785	3.763	1.000	0.996	0.944	0.952
		Theory	3.862	3.862	1.000	1.000	0.965	0.965
	DH	FEM	11.270	1.267	0.334	2.964	1765.21	1784.08
		Theory	11.570	1.287	0.333	2.995	1809.99	1809.99
ZPR	SREH	FEM	5.632	794.409	2.628e-6	1.845e-8	0.617	0.621
		Theory	5.785	805.085	0	0	0.643	0.643
	FPSH	FEM	6.506	6.576	1.427e-4	1.415e-4	0.272	0.275
		Theory	6.680	6.680	0	0	0.279	0.279
NPR	REH	FEM	3.788	3.956	-1.024	-0.972	0.143	0.143
		Theory	3.862	3.862	-1.000	-1.000	0.145	0.145
	DAH	FEM	5.910	6.153	-1.013	-0.971	573.05	579.23
		Theory	6.164	6.164	-1.000	-1.000	NA	NA

Appendix B. Tables for the imperfection sensitivity coefficients

Table A2
The imperfection sensitivity coefficients for different lattice materials when the imperfection fraction $f = 1$ %.

Lattice		$S_{E_{11}}^{0.01}$	$S_{E_{22}}^{0.01}$	$S_{G_{12}}^{0.01}$	$S_{\nu_{21}}^{0.01}$	$S_{\nu_{12}}^{0.01}$
PPR	HH	0.084	0.081	0.053	0.0637	0.0605
	DH	0.016	0.016	0.491	0.0011	0.0011
ZPR	SREH	0.072	0.982	0.023	2.709E-02	7.611E-02
	FPSH	0.046	0.042	0.025	1.635E-04	1.651E-04
NPR	REH	0.137	0.169	0.026	0.1516	0.1833
	DAH	0.043	0.126	0.952	0.0657	0.1468

Table A3
The imperfection sensitivity coefficients for different lattice materials when the imperfection fraction $f = 10$ %.

Lattice		$S_{E_{11}}^{0.1}$	$S_{E_{22}}^{0.1}$	$S_{G_{12}}^{0.1}$	$S_{\nu_{21}}^{0.1}$	$S_{\nu_{12}}^{0.1}$
PPR	HH	0.622	0.633	0.521	0.4698	0.4847
	DH	0.200	0.201	0.983	0.0500	0.0509
ZPR	SREH	0.582	0.999	0.456	2.018E-01	7.650E-02
	FPSH	0.425	0.429	0.242	3.281E-03	3.280E-03
NPR	REH	0.782	0.793	0.314	0.8913	0.8968
	DAH	0.401	0.696	0.997	0.6442	0.8196

Appendix C. Supplementary material

Supplementary data to this article can be found online at https://doi.org/10.1016/j.compositesa.2025.109215.

Data availability

Data will be made available on request.

References

[1] Pan C, Han Y, Lu J. Design and optimization of lattice structures: a review. Appl Sci 2020;10(18).
[2] Pan F, Li Y, Li Z, Yang J, Liu B, Chen Y. 3D pixel mechanical metamaterials. Adv Mater 2019;31(25).
[3] Liu W, Song H, Huang C. Maximizing mechanical properties and minimizing support material of PolyJet fabricated 3D lattice structures. Addit Manuf 2020;35.
[4] Wang K, Chang YH, Chen Y, Zhang C, Wang B. Designable dual-material auxetic metamaterials using three-dimensional printing. Mater Des 2015;67:159–64.
[5] Sang L, Han S, Peng X, Jian X, Wang J. Development of 3D-printed basalt fiber reinforced thermoplastic honeycombs with enhanced compressive mechanical properties. Composites, Part A. 2019;125.
[6] Dong K, Wang Y, Wang Z, Qiu W, Zheng P, Xiong Y. Reusability and energy absorption behavior of 4D printed continuous fiber-reinforced auxetic composite structures. Composites, Part A. 2023;169.
[7] Ruan K, Peng Y, Weng Y, Zhou L, Xiong Y. Rotatory additive manufacturing of grid-stiffened continuous fiber-reinforced polymer tubular structures. Composites, Part A. 2025;194.
[8] Huang C, Chen L. Negative Poisson's ratio in modern functional materials. Adv Mater 2016;28(37):8079–96.
[9] Qiu XM, Zhang J, Yu TX. Collapse of periodic planar lattices under uniaxial compression, part II: Dynamic crushing based on finite element simulation. Int J Impact Eng 2009;36(10–11):1231–41.
[10] Huo YZ, Yang JS, Suo Z, Zhao T, Wang WJ, Tong YH, et al. Low velocity impact response of carbon fiber reinforced thermoplastic composite honeycomb sandwich structure considering mesoscopic damage behavior. Composites, Part A. 2025;194.
[11] Hua L, Ding L, Wang X, Zeng S, Huang H, Liang X, et al. Out-of-plane energy absorption of 3D printed basalt-fiber-reinforced hierarchical honeycomb composite. Int J Mech Sci 2025;285.
[12] Wang Y, Wei X, Li Z, Gong C, Xue P, Xiong J. Low-velocity impact responses and failure of sandwich structure with carbon fiber composite honeycomb cores. Int J Impact Eng 2024;192.
[13] Zhang R, Wang Y, Wei X, Xiong J. Experimental and numerical study of high-velocity impact behavior of carbon fiber honeycomb sandwich structures. Int J Impact Eng 2025;206.
[14] Flora F, Boccaccio M, Pinto F, Meo M. A bistable impact resistant sandwich carbon-fibre reinforced core. Compos Struct 2024;331.
[15] Lu J, Li Q, Qin R, Wang X, Li T, Niu H, et al. Enhanced energy absorption of assembled honeycomb system under in-plane compression. Int J Mech Sci 2025;299.
[16] Wang W, Liu S, Zhou J, Li Z, Zhang J, Mei G, et al. A rate-dependent shape memory polymer composite for self-folding 2D-to-3D structural transition with improved impact resistance. Composites, Part B. 2025;297.
[17] Montazeri A, Saeedi A, Bahmanpour E, Safarabadi M. Heterogeneous hexagonal honeycombs with nature-inspired defect channels under in-plane crushing. Mater Lett 2024;366.
[18] Cai Z, Deng X, Huang C, Xie Z. Crashworthiness analysis of a novel bioinspired hexagonal honeycomb under out-of-plane crushing. Mech Adv Mater Struct 2023;31(25):6676–95.
[19] Del Broccolo S, Laurenzi S, Scarpa F. AUXHEX – a Kirigami inspired zero Poisson's ratio cellular structure. Compos Struct 2017;176:433–41.
[20] Virk K, Monti A, Trehard T, Marsh M, Hazra K, Boba K, et al. SILICOMB PEEK Kirigami cellular structures: mechanical response and energy dissipation through zero and negative stiffness. Smart Mater Struct 2013;22(8).
[21] Olympio KR, Gandhi F. Zero Poisson's Ratio Cellular Honeycombs for Flex Skins Undergoing One-Dimensional Morphing. J Intell Mater Syst Struct 2009;21(17):1737–53.
[22] Rong J, Zhou L. Study of a zero Poisson's ratio honeycomb used for flexible skin. Mater Res Express 2017;4(4).
[23] Zou T, Zhou L. Mechanical property analysis and experimental demonstration of zero Poisson's ratio mixed cruciform honeycomb. Mater Res Express 2017;4(4).
[24] Chen J, Shen X, Li J. Zero Poisson's ratio flexible skin for potential two-dimensional wing morphing. Aerosp Sci Technol 2015;45:228–41.
[25] Grima JN, Oliveri L, Attard D, Ellul B, Gatt R, Cicala G, et al. Hexagonal Honeycombs with Zero Poisson's Ratios and Enhanced Stiffness. Adv Eng Mater 2010;12(9):855–62.
[26] Attard D, Grima JN. Modelling of hexagonal honeycombs exhibiting zero Poisson's ratio. physica status solidi (b). 2010;248(1):52-9.
[27] Soman P, Fozdar DY, Lee JW, Phadke A, Varghese S, Chen S. A three-dimensional polymer scaffolding material exhibiting a zero Poisson's ratio. Soft Matter 2012;8(18).
[28] Huang J, Liu W, Tang A. Effects of fine-scale features on the elastic properties of zero Poisson's ratio honeycombs. Mater Sci Eng B 2018;236–237:95–103.
[29] Wu Z, Zhao J, Wu W, Wang P, Wang B, Li G, et al. Radial compressive property and the proof-of-concept study for realizing self-expansion of 3D printing polylactic acid vascular stents with negative poisson's ratio structure. Materials 2018;11(8).
[30] Douglas GR, Phani AS, Gagnon J. Analyses and design of expansion mechanisms of balloon expandable vascular stents. J Biomech 2014;47(6):1438–46.
[31] Tan TW, Douglas GR, Bond T, Phani AS. Compliance and longitudinal strain of cardiovascular stents: influence of cell geometry. J Med Devices 2011;5(4).
[32] Kapnisi M, Mansfield C, Marijon C, Guex AG, Perbellini F, Bardi I, et al. Auxetic cardiac patches with tunable mechanical and conductive properties toward treating myocardial infarction. Adv Funct Mater 2018;28(21).
[33] Chow L, Kl Y, Wong KH, Leung MS, Sun Y, My K, et al. 3D printing auxetic architectures for hypertrophic scar therapy. Macromol Mater Eng 2022;307(5).
[34] Mao L, Pan T, Ke Y, Yan Z, Huang S, Guo D, et al. Configurable direction sensitivity of skin-mounted microfluidic strain sensor with auxetic metamaterial. Lab Chip 2022;22(8):1630–9.
[35] Kolken HMA, Garcia AF, Du Plessis A, Rans C, Mirzaali MJ, Zadpoor AA. Fatigue performance of auxetic meta-biomaterials. Acta Biomater 2021;126:511–23.
[36] Kolken HMA, Garcia AF, Plessis AD, Meynen A, Rans C, Scheys L, et al. Mechanisms of fatigue crack initiation and propagation in auxetic meta-biomaterials. Acta Biomater 2022;138:398–409.
[37] Kolken HMA, Lietaert K, van der Sloten T, Pouran B, Meynen A, Van Loock G, et al. Mechanical performance of auxetic meta-biomaterials. J Mech Behav Biomed Mater 2020;104.
[38] Carneiro V, Puga H. Modeling and elastic simulation of auxetic magnesium stents. 2015 IEEE 4th Portuguese Meeting on Bioengineering (ENBENG): IEEE; 2015. p. 1-4.
[39] Silva MJ, Gibson LJ. The effects of non-periodic microstructure and defects on the compressive strength of two-dimensional cellular solids. Int J Mech Sci 1997;39(5):549–63.
[40] Simone A, Gibson L. Effects of solid distribution on the stiffness and strength of metallic foams. Acta Mater 1998;46(6):2139–50.
[41] Simone A, Gibson L. The effects of cell face curvature and corrugations on the stiffness and strength of metallic foams. Acta Mater 1998;46(11):3929–35.
[42] Guo XE, Gibson LJ. Behavior of intact and damaged honeycombs: a finite element study. Int J Mech Sci 1999;41(1):85–105.
[43] Chen C, Lu TJ, Fleck NA. Effect of imperfections on the yielding of two-dimensional foams. J Mech Phys Solids 1999;47(11):2235–72.
[44] Li K, Gao XL, Subhash G. Effects of cell shape and cell wall thickness variations on the elastic properties of two-dimensional cellular solids. Int J Solids Struct 2005;42(5–6):1777–95.
[45] Symons DD, Fleck NA. The imperfection sensitivity of isotropic two-dimensional elastic lattices. J Appl Mech 2008.
[46] Zhang XC, Liu Y, Wang B, Zhang ZM. Effects of defects on the in-plane dynamic crushing of metal honeycombs. Int J Mech Sci 2010;52(10):1290–8.
[47] Romijn NE, Fleck NA. The fracture toughness of planar lattices: Imperfection sensitivity. J Mech Phys Solids 2007;55(12):2538–64.
[48] Tankasala HC, Deshpande VS, Fleck NA. Tensile response of elastoplastic lattices at finite strain. J Mech Phys Solids 2017;109:307–30.
[49] Liu W, Wang N, Huang J, Zhong H. The effect of irregularity, residual convex units and stresses on the effective mechanical properties of 2D auxetic cellular structure. Mater Sci Eng A 2014;609:26–33.
[50] Evans KE, Nkansah MA, Hutchinson IJ. Auxetic foams: modelling negative Poisson's ratios. Acta Metall Mater 1994;42(4):1289–94.
[51] Gibson LJ, Ashby MF. Cellular solids: Structure & properties. Pergamon Press, Oxford; 1988.
[52] Gong X, Huang J, Scarpa F, Liu Y, Leng J. Zero Poisson's ratio cellular structure for two-dimensional morphing applications. Compos Struct 2015;134:384–92.
[53] Karathanasopoulos N, Dos Reis F, Reda H, Ganghoffer JF. Computing the effective bulk and normal to shear properties of common two-dimensional architectured materials. Comput Mater Sci 2018;154:284–94.
[54] Yang H, Wang B, Ma L. Designing hierarchical metamaterials by topology analysis with tailored Poisson's ratio and Young's modulus. Compos Struct 2019;214:359–78.
[55] Deshpande V, Ashby M, Fleck N. Foam topology: bending versus stretching dominated architectures. Acta Mater 2001;49(6):1035–40.
[56] Maxwell JC. On the calculation of the equilibrium and stiffness of frames. The London, Edinburgh, and Dublin Philosophical Magazine and Journal of Science 1864;27(182):294-9.
[57] Chen Y, Pan F, Guo Z, Liu B, Zhang J. Stiffness threshold of randomly distributed carbon nanotube networks. J Mech Phys Solids 2015;84:395–423.